Emergence of microstructure and oxygen diffusion in yttrium-stabilized cubic zirconia

C. Yang,[1,*] K. Trachenko,[1] S. Hull,[2] I. T. Todorov,[3] and M. T. Dove[1,4,†]

[1]*School of Physics and Astronomy, Queen Mary University of London, Mile End Road, London, E1 4NS, United Kingdom*

[2]*ISIS Facility, Rutherford Appleton Laboratory, Chilton, Oxfordshire, OX11 0QX, United Kingdom*

[3]*STFC Daresbury Laboratory, Warrington WA4 1EP, United Kingdom*

[4]*School of Physical Science and Technology, Sichuan University, Chengdu 610065, People's Republic of China*

(Received 24 July 2017; revised manuscript received 15 January 2018; published 29 May 2018)

Large-scale molecular dynamics simulations have been used to study the microstructure in Y-doped ZrO_2. From simulations performed as a function of composition the dependence of microstructure on composition is quantified, showing how it is formed from two coexisting phases, and the transformation to the stabilized cubic form is observed at higher concentrations of yttrium and higher temperatures. The effect of composition and temperature on oxygen diffusion is also studied, showing strong correlations between microstructure and diffusion.

DOI: 10.1103/PhysRevB.97.184107

I. INTRODUCTION

Zirconia (ZrO_2) is an important industrial material. Owing to its high oxygen ion conductivity, it finds many applications, for example, in oxygen sensors, solid-oxide fuel cells, and catalytic sensors. These applications are for the cubic phase of ZrO_2, which can be made by doping the structure with high concentrations of yttrium. Since the formal charge of yttrium is +3 and zirconium is +4, oxygen is removed when zirconium is replaced by yttrium so as to preserve charge balance, which allows high oxygen diffusion [1–3].

There have been many studies focused on the phase stability of Y-doped ZrO_2 [1,2,4–7]. At room temperature, the crystal structure of pure ZrO_2 is monoclinic. It transforms to the phase of tetragonal symmetry at 1170 °C and cubic symmetry at 2370 °C. However, ZrO_2 also forms a stable cubic phase when it is doped with a high concentration of divalent or trivalent cations and a metastable tetragonal phase with a low concentration of divalent or trivalent cations at room temperature. The metastable tetragonal structure slowly transforms to the stable monoclinic structure at low temperature (∼400 K). Chevalier *et al.* [1] collected a wide range of data for both the metastable and stable phase diagram of Y-doped ZrO_2. In the metastable phase diagram, there is a metastable tetragonal phase existing for concentrations of 8–18% at room temperature. In the stable phase diagram, ZrO_2 forms a cubic phase when the concentration of yttrium reaches 20% at room temperature.

Experimentally, both Kim *et al.* [7] and García-Martín *et al.* [6] observed the domains of different phases coexisting in ZrO_2 with 3.2% and 8% of Y_2O_3 by transmission electron microscopy. However, the challenge of experimental study of these microstructures is that yttrium could be unevenly distributed in the material due to low cation diffusion, and cubic structures tend to form in high Y-concentrated regions [2]. Since microstructure may play an important role in oxygen diffusion, it is essential to study how microstructure emerges and evolves in detail.

There has been only a small number of simulation studies focusing on the microstructure during phase transformation. Most of these have used relatively small sizes of atomic configurations, which means it would be impossible to include the naturally emerging microstructure [8–10]. The studies which included microstructure typically created artificial grains, for example, by using the Voronoi tessellation method [11]. With recent developments in computer technologies and associated simulation software it is now appropriate to study the changes of microstructure of Y-doped ZrO_2 formed "naturally" using molecular dynamics (MD) simulations with very large configuration sizes.

On the other hand, there have been numerous diffusion studies on Y-stabilized ZrO_2, because many applications are based on its diffusion property. Most experimental studies show that the activation energy of oxygen exhibits an almost linear correlation with the concentration of yttrium [12–17]. Interestingly, the activation energy of oxygen diffusion also changes with temperature [14,15,18]. The reason for this phenomenon is still unclear. In comparison, the results of simulation studies show a more complicated and unclear trend with concentration of yttrium [12,13,19,20], but as we noted these have not been able to include the effects of naturally forming microstructures.

In this study, our aim has been to develop a model that can simulate the microstructure transformation during the monoclinic-cubic transition of Y-stabilized ZrO_2. We performed extensive MD simulations for ZrO_2 in a wide range of yttrium concentrations. The system size was extended up to 360 Å of the supercell size. We directly observed the emergence of microstructure of two different phases, albeit with a stable orthorhombic rather than monoclinic phase. Up to yttrium

*Present address: Institute of Natural Sciences and Department of Physics and Astronomy, Shanghai Jiao Tong University, Shanghai 200240, People's Republic of China.

†martin.dove@qmul.ac.uk

TABLE I. Fitted Buckingham parameters and the charge of O, Zr and Y for ZrO_2.

	A (eV)	ρ (Å)	C (eV Å^6)	Charge (| e |)
O–O	1071	0.3623	175	−1.2
Zr–O	7375	0.2265	0.0	2.4
Y–O	181110	0.1726	0.0	1.8

concentrations of around 10% the cubic phase exists around the interface regions, whereas around 10–18% we observed a mixture of both phases across the whole sample. Above a concentration of around 18% only the cubic phase is stable and the microstructure disappears. Although the simulations see the orthorhombic rather than monoclinic phase, nevertheless the emergent microstructure is closely representative of what is seen in experimental data, together with the observation of a phase transition to the cubic form stabilized at higher concentrations of yttrium. Here we first report results from the simulation that quantify the formation of the microstructure. Second we report results on the dependence of oxygen diffusion on concentration, and observe correlations with both the formation of microstructure and transformation to the cubic phase.

II. METHODS

A. Interatomic potential for yttrium-doped zirconia

We have developed a model for ZrO_2 based on the use of Buckingham potential functions, with final values shown as in Table I.

$$U(r_{ij}) = A\exp(-r_{ij}/\rho) - C/r_{ij}^6. \quad (1)$$

We fitted the parameters in the model interatomic potential against the simulated energies from DFT calculations [8], crystal structures, and experimental data for elastic constants [21], using the GULP program [22]. The comparison of the values of the elastic constants calculated by our proposed model and that of Schelling [10], and with experimental data [21], is given in Table II. It can be seen that our model gives a better result for the Y-stabilized cubic phase, and Schelling's model gives a better result for the tetragonal phase. Similar to other ZrO_2 studies based on empirical potentials, our model suffers from the problem that the structure of ZrO_2 prefers to form the orthorhombic phase rather than the lower-symmetry monoclinic phase. Although this means that MD simulations will not generate the monoclinic phase, we are still able to observe the transformation of microstructure during the phase transition. We consider that the orthorhombic phase plays the same role as the monoclinic phase in terms of formation and evolution of a naturally emerging microstructure.

TABLE II. Comparison of elastic constants (GPa) for ZrO_2 by using our model, Schelling's model [10], and experiment results [21].

	Our model	Schelling model	Experiment
C_{11}(cubic)	391	664	402
C_{12}(cubic)	69	104	95
C_{44}(cubic)	68	98	56
C_{11}(tetragonal)	276	523	451
C_{12}(tetragonal)	159	270	240
C_{44}(tetragonal)	9	58	39

B. Details of molecular dynamics simulations

Simulation samples were produced starting with the cubic phase of ZrO_2, with zirconium atoms chosen at random to be replaced by yttrium, with randomly selected oxygen atoms removed from the configurations to ensure the charge balance. MD simulations were performed using DL_POLY [23] to simulate the structure and oxygen diffusion for Y-stabilized ZrO_2 with 0–25% of yttrium. The configuration sizes varied from 96 000–4 116 000 atoms, with configuration edge sizes of 100–360 Å. All structures were equilibrated at 2000 K, and the temperature was decreased slowly to 300 K at a rate 2 K ps in MD simulations. The equilibration was performed in the constant-temperature and constant-stress ensemble, which allows both the volume and shape of the simulation box to change during the simulation. A time step of 0.001 ps was used for all simulations.

C. Cation coordination

Different crystallographic phases in the ZrO_2-Y_2O_3 system have different cation coordination numbers. This allows us to identify different phases based on the cation environment. However, since there are naturally formed oxygen vacancies in yttrium-doped zirconia, we analyze the cation-cation coordination instead of cation-anion coordination to distinguish two phases. In both phases the nearest neighbor cations form a dodecahedron, as shown in Fig. 1 for both cubic and orthorhombic phases. The angle and distance distributions of the dodecahedra found in the simulation can be used to determine the phase of the local structure seen by any cation. Figure 2 shows the angle and distance distributions calculated from pure ZrO_2 and $Zr_{0.8}Y_{0.2}O_{1.9}$. These are used as a baseline for separating the two phases shown in Fig. 1. For the analysis of the dodecahedra we developed bespoke software to calculate distances and angles for each dodecahedron and then check that the distribution fits the range of each peak in the baseline. Since the distribution of the peaks of angles overlap each other in the orthorhombic structure, the peaks cannot be differentiated easily. For this reason the angles were divided into three scenarios: *first*, the interior angles of the triangle faces of the

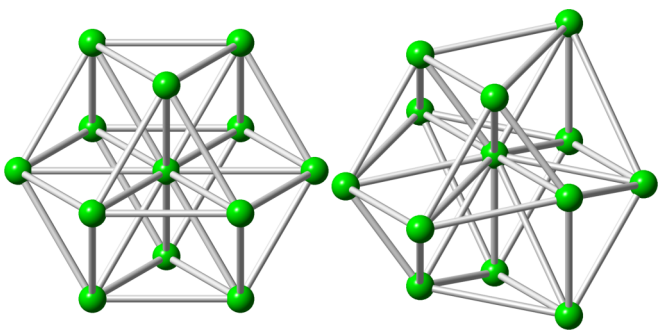

FIG. 1. Cation and its coordination cation for cubic (left) and orthorhombic (right) phases.

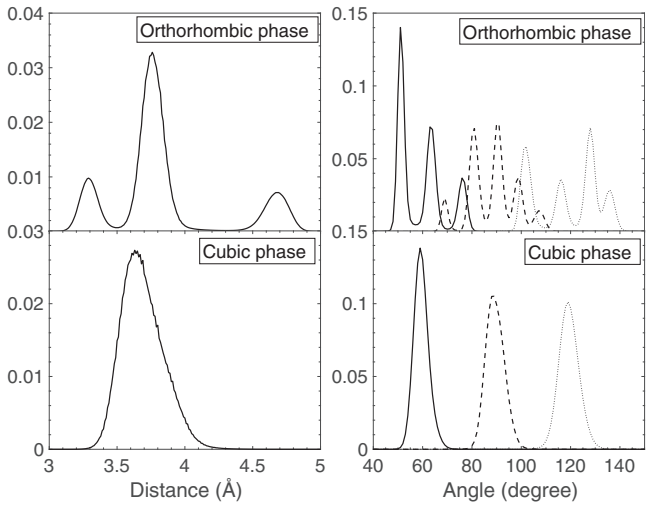

FIG. 2. Cation-cation distance (left) and angle (right) distribution of dodecahedrons for cubic and orthorhombic phases. The angle distribution is divided into three scenarios: (a) the interior angles of the triangle faces of the dodecahedra (solid line), (b) the interior angles of the quadrilateral faces of the dodecahedra (dash line), (c) other angles formed by the edges of the dodecahedra (dot line).

dodecahedra; *second*, the interior angles of the quadrilateral faces of the dodecahedra; and *third*, other angles formed by the edges of the dodecahedra, which the peak position equals 60°, 90°, and 120° in cubic structure respectively. Thus, the range of angles can be separated in these different scenarios.

III. RESULTS AND DISCUSSION

A. Microstructure transformations in yttrium-stabilized cubic zirconia

1. Phase transition of ZrO_2 caused by doping with Y

Figure 3 shows that microstructures form with increasing concentration of yttrium. In our simulation, this does not generate a significant change of the shape of the simulation samples, which remain cubic after the annealing processes. The system without yttrium forms the orthorhombic phase with different orientations, but we can still observe a small amount of the cubic phase existing in the grain boundary between orthorhombic grains. When the concentration of yttrium reaches 20%, the system transforms to the cubic structure. Between 0 and 20%, both cubic and orthorhombic phases coexist in the system, and the concentration of the cubic

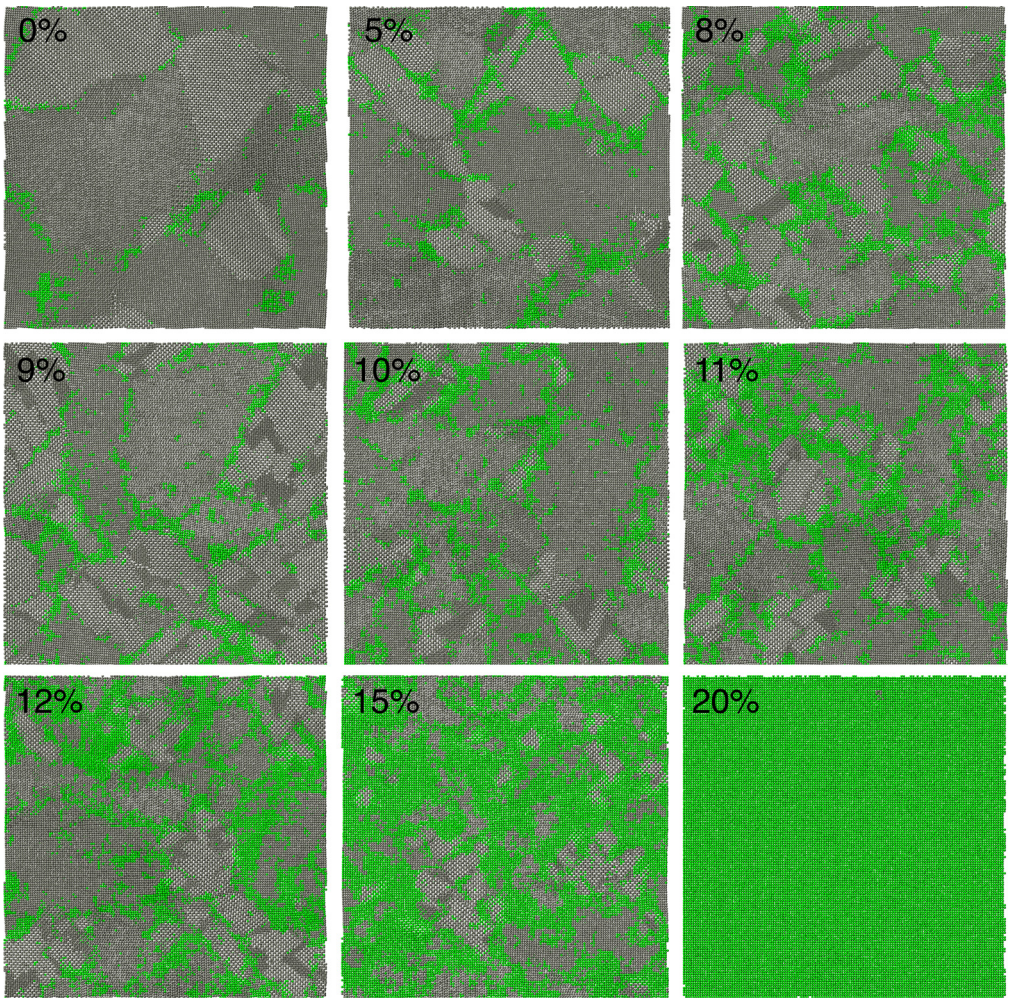

FIG. 3. Microstructure of the cubic phase (green) coexisting with the orthorhombic phase (gray) at different concentrations of yttrium in the formula with 1 372 000 cations and cell size around 360 Å. We only show cations in the structure. The cubic phase is seen to grow in the system with increasing concentration of yttrium.

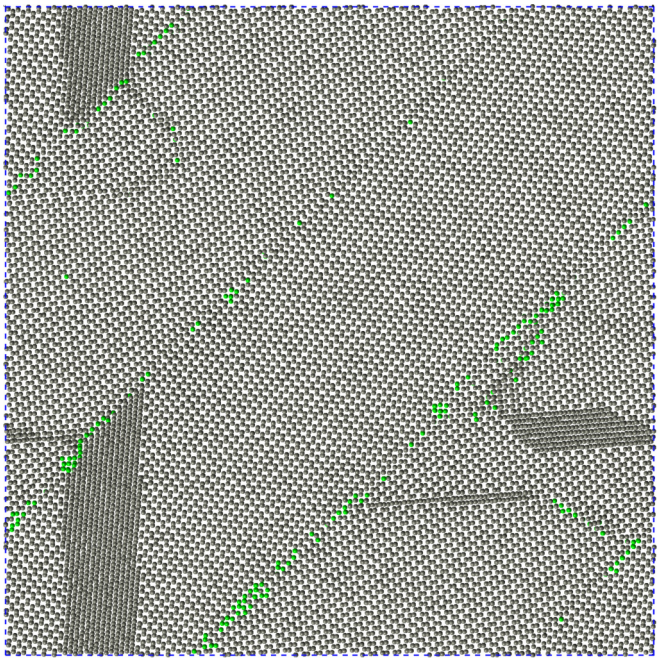

FIG. 4. Microstructure of the cubic phase (green) and orthorhombic phase (gray) for ZrO_2 with 864,000 cations and the cell size around 310 Å. The orthorhombic phase align along a specific direction if the system size is too small.

phase increases with the concentration of yttrium. Similar microstructure was also observed in experimental studies [6].

While it is obviously necessary to use very large atomic configurations to simulate the formations of microstructures, our work shows that the finite size effect still affects the simulation in a very large system. For example, in Fig. 4 we show how a configuration consisting of 864 000 cations with configuration edge length of around 310 Å has most of the crystalline structure aligning to a specific orientation. However, this does not happen in a configuration consisting of 1 372 000 cations with the configuration edge length of about 360 Å. This indicates that the behavior of the simulation can still be affected by finite size effects up to 360 Å.

Since yttrium atoms are randomly distributed in the system, we can study the relationship between the formation of the cubic phase and the local concentration of yttrium atoms. In Fig. 5, we plot the proportion of yttrium in the cubic cluster. As can be seen in Fig. 5, before the structure completely transforms to the cubic phase, the concentration of yttrium in the cubic domain is around 25% higher than the concentration of yttrium in the system. This confirms that the cubic phase domains prefer to form in high-yttrium concentration regions.

To quantify this transformation, we calculated the concentration of cations in the cubic phase with four different system sizes shown in Fig. 6. There appears to be a large fluctuation in the system consisting of $Zr_{1-x}Y_xO_{2-x/2}$ with 32 000 cations and a configuration size of around 105 Å, but the result becomes more consistent with larger system sizes. For the concentration of yttrium between 0 and 9%, the concentration of the cubic phase increases gradually and linearly with the increase in yttrium. In this case the cubic phase was growing within and around the grain boundaries. After 10% yttrium concentration

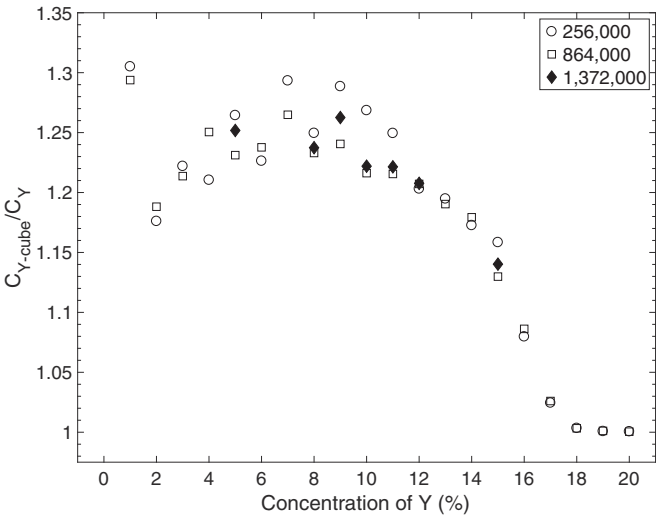

FIG. 5. Concentration of yttrium in the cubic domain divided by concentration of yttrium in the system.

the concentration of the cubic phase in the sample increases rapidly, and reaches saturation after 18% yttrium.

The rapid transformation to the cubic form is also reflected in the volume of the configuration. Figure 7 shows the linear size as $V^{\frac{1}{3}}$ scaled to represent one unit cell. It can be seen that the volume increases slightly with the concentration of yttrium before 10% of yttrium due to the fact that the ion size of yttrium is larger than zirconium, and then the volume starts to decrease rapidly with yttrium concentration. After 20%, the volume starts to increase again with concentration. The volume of ZrO_2 without yttrium and with 20% of yttrium corresponds to the volume of orthorhombic and cubic phases of ZrO_2, respectively.

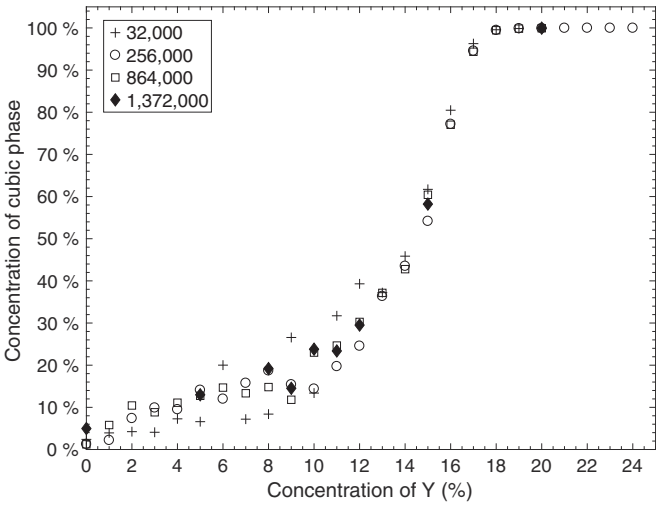

FIG. 6. Concentration of the cubic phase for different system sizes vs concentration of yttrium. Concentration of the cubic phase increases with the concentration of yttrium.

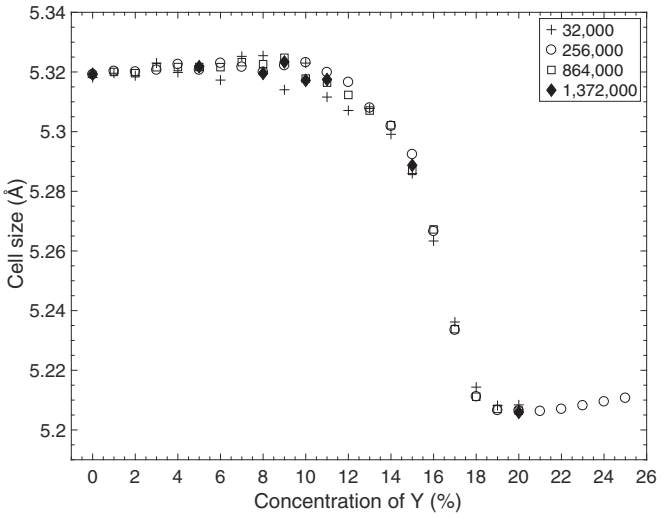

FIG. 7. Cell size ($V^{\frac{1}{3}}$) for different system sizes vs concentration of yttrium. A phase transition occurs at around 10% of yttrium.

2. Grain size changes through the transition

To quantify the grain size, we calculated the correlation function $g(r) = \langle S(0) \cdot S(r) \rangle$, where $S(r)$ is defined as

$$\begin{aligned} S(r) &= 0 \text{ site of the orthorhombic phase,} \\ S(r) &= 1 \text{ site of the cubic phase,} \end{aligned} \tag{2}$$

and the starting point is always from sites in the cubic phase. It can be seen from Fig. 8 that the correlation function decays from 1 to the concentration of the cubic phase. The correlation function is fitted by

$$g(r) = (1 - c)\exp(-r/\xi) + c, \tag{3}$$

where c is the concentration of the cubic phase, and ξ is the correlation length.

To calibrate the relationship between the correlation length and grain size, we constructed artificial cubic boxes with fixed

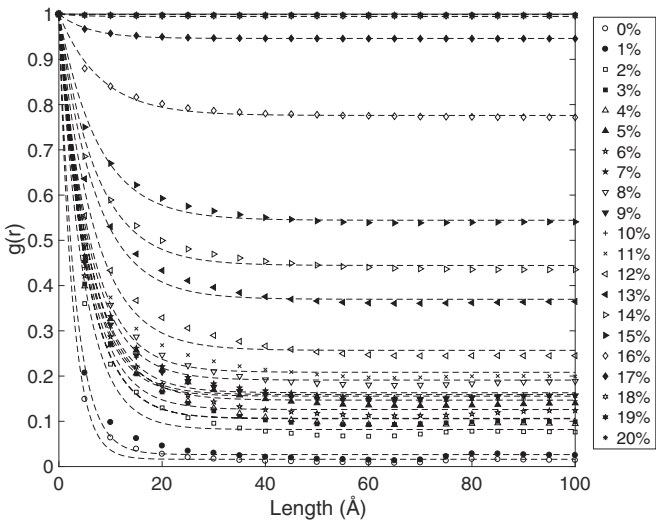

FIG. 8. Correlation function of the cubic phase of the ZrO_2 with 0–20% of yttrium.

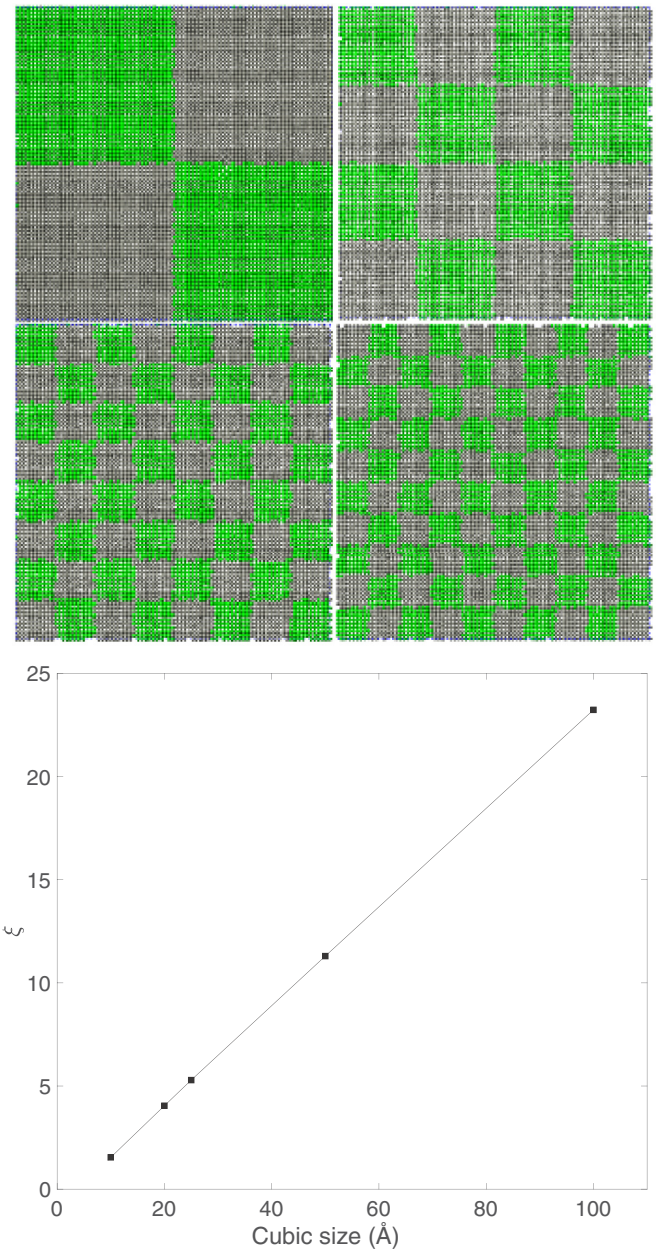

FIG. 9. Top: Examples of artificial systems containing cubic boxes with same size. Bottom: Cube edge length vs correlation parameter ξ, showing a linear relationship between them.

size in the system as shown in Fig. 9 (top). Since the exact sizes of the regions of the cubic phase are known, the relationship between the correlation length and size of the cubic phase is plotted in Fig. 9 (bottom). The grain size shown is calculated by scaling the correlation length using the relationship between the size and ξ shown in Fig. 10.

Figure 10 shows the grain size of the microstructures. It can be seen that the fluctuations are larger for the $Zr_{1-x}Y_xO_{2-x/2}$ with 32 000 cations. It is also seen that at low yttrium concentration, the microstructure is affected more by the simulation size. When the concentration of yttrium is above 15%, the grain sizes for different size configurations above 256 000 cations are consistent with each other. For the $Zr_{1-x}Y_xO_{2-x/2}$ system

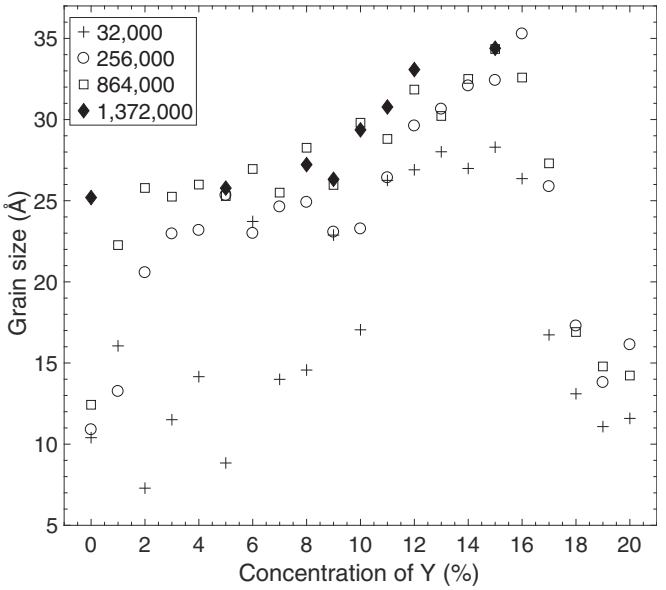

FIG. 10. Grain size vs concentration of yttrium for systems with different size.

with 1 372 000 cations, the grain size does not change for low concentrations of yttrium until the phase transition occurs. After the phase transition, the grain size starts to increase again, although this trend is different in the smaller system. In this case the grain size in the smaller system increases at the beginning, then becomes flat and increases again after the phase transition. This is likely to be caused by the specific orientation of the orthorhombic phase shown in Fig. 4.

In summary, the structural properties are influenced to various extents by the finite size effect. The shape and size of grains show stronger finite size effects than other structural properties shown in Figs. 3 and 4, which results in the dependence of grain size at low concentration of yttrium on configuration size. Other properties such as concentration of cubic phase and cell size are less affected by the system size.

B. Oxygen vacancy distribution

An experimental study of the diffuse scattering in yttrium-doped zirconia [5] has confirmed that oxygen vacancy pairs form along cation centered [1 1 1] fluorite direction. Oxygen vacancy distribution can affect the pathway of oxygen diffusion. Thus before studying oxygen diffusion, it is important to check if our model can reproduce correctly the oxygen vacancies distribution.

The oxygen vacancies were located using the criterion defined in Ref. [17]. Every four closest cations form a tetrahedron structure. If there is no oxygen atom in the tetrahedron, the center of the tetrahedron is defined as the position of a vacancy. In our simulations, there are oxygen atoms with large displacement located just outside of the tetrahedra. The oxygen-vacancy pair distribution function is plotted in Fig. 11.

The vacancy-vacancy pair distribution in $Zr_{1.8}Y_{0.2}O_{1.9}$ at room temperature is compared with that from a system with an initial random distribution in Fig. 12. It shows that the cation-centered oxygen vacancy pairs prefer to form along ⟨111⟩ directions. This result is in agreement with the diffuse

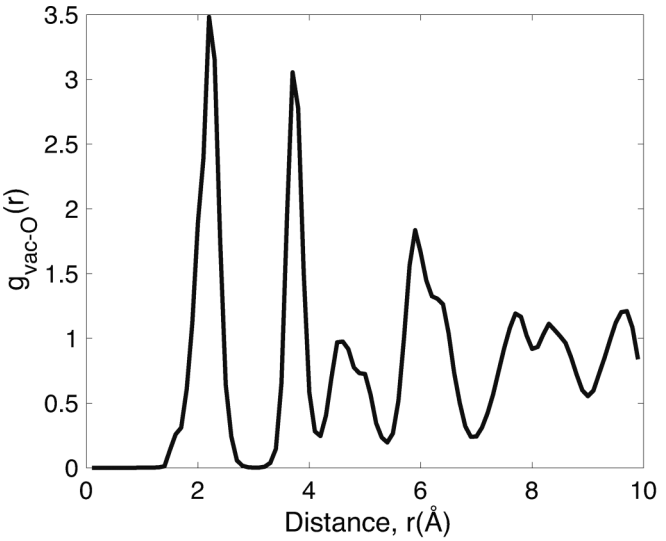

FIG. 11. Pair distribution function for $Zr_{0.8}Y_{0.2}O_{1.9}$ between oxygen atoms and oxygen vacancies at room temperature.

scattering experiment result, which shows vacancy pairs form along ⟨111⟩ fluorite directions in ZrO_2 with high concentrations of yttrium [5]. In our simulation, 89% of cation-centered oxygen vacancy pairs are along the ⟨111⟩ fluorite directions, 10% along ⟨110⟩, and less than 1% along the ⟨100⟩ directions at room temperature.

C. Oxygen diffusion in yttrium-stabilized cubic zirconia

In this part we report calculations of the diffusion coefficient D for $Zr_{1-x}Y_xO_{2-x/2}$ for wide variations in both yttrium concentration x and temperature T. Calculations of D have been obtained from the time dependence of the mean-square displacements of different atom types in the simulation,

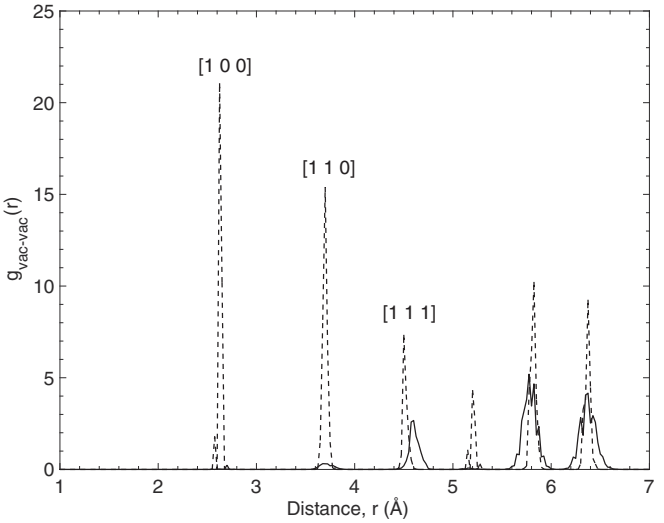

FIG. 12. Pair distribution function for $Zr_{0.8}Y_{0.2}O_{1.9}$ between oxygen vacancies at room temperature. The solid line is the distribution at room temperature obtained from simulation and the dashed line has been calculated by assuming a random distribution of oxygen vacancies.

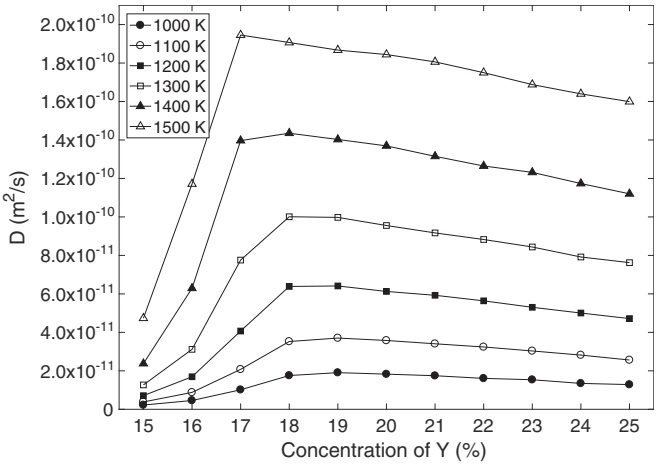

FIG. 13. Diffusion coefficient D of oxygen vs concentration of yttrium for several different temperatures. The maximum in the diffusion coefficient occurs for yttrium concentrations between 17% and 19%.

namely, from $D = \langle r^2 \rangle / 6t$, where time t ran to 100 ps. Diffusion calculations were performed using samples with 256 000 cations and a cell size around 200 Å, which was shown from the results above to be large enough to avoid size effects in the formation of microstructure, but small enough to enable the many calculations required to be practical. Constant-energy and constant-volume simulations were used for this part of the study.

In Fig. 13, the diffusion coefficient of oxygen calculated from the mean-squared atomic displacement is plotted against the concentration of yttrium at a temperature range between 1000 and 1500 K. This result is in good agreement with experiment results [12,24]. We also noticed that the concentration of the maximum in D increases slightly with decreasing temperature in our model. Although this result differs from what has been seen in other experimental studies [17,24], the data are not extensive in those studies. Thus it would be desirable to perform more extensive experimental studies to determine better the variation of the maximum in the diffusion coefficient with concentration.

Figure 14 shows plots of $\ln D$ vs $1/T$ for many yttrium concentrations. The upper graph shows that for most concentrations the relationship is close to linear, and for yttrium concentrations above 20% the slopes are very similar. The lower graph shows that for lower concentrations (in this case 17% and 18% yttrium) the relationship between $\ln D$ and $1/T$ is not constant over the range of temperatures when extended to 2000 K. At higher temperature the slope becomes similar to that for high concentration of yttrium, and at such temperature the structure transforms to a cubic phase. This transformation is seen in Fig. 15, which shows the structure of ZrO_2 with 16% of yttrium at 1000 and 1800 K. These results suggest that the effective activation energy of oxygen diffusion is higher in the mixed cubic and orthorhombic states. This may explain the changes of activation energy observed in experiment studies [14,15,18].

To develop the point further, in Fig. 16 we show the effective activation energy of oxygen diffusion for $Zr_{1-x}Y_xO_{2-x/2}$

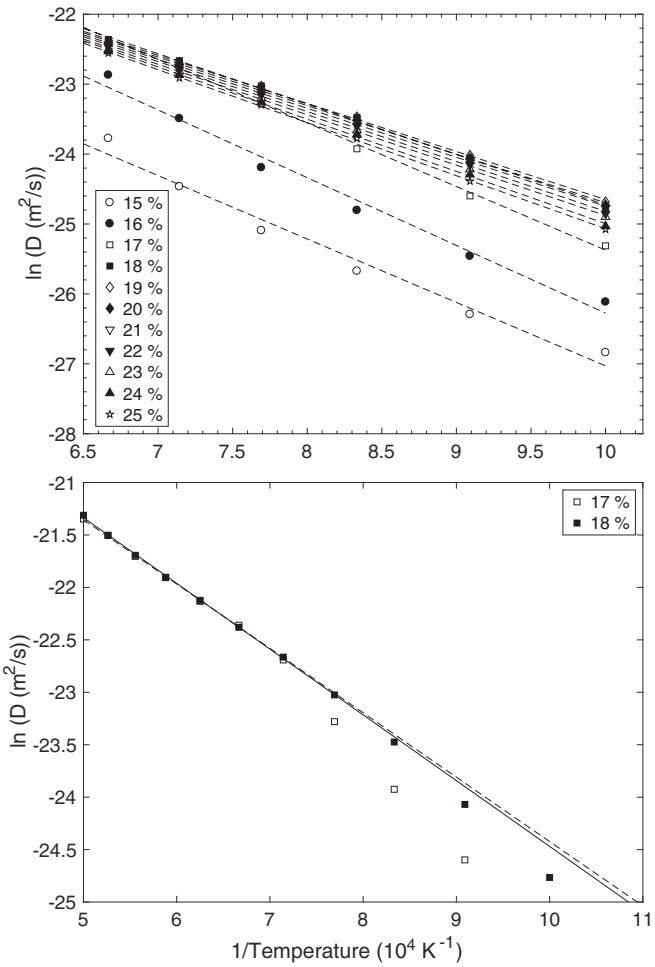

FIG. 14. Top: $\ln D$ vs $1/T$ for different concentrations of yttrium. Bottom: Examples that slope changes with temperature for yttrium concentrations of 17% and 18%.

extracted from the diffusivity data for both mixed-phase configurations with microstructure (filled squares, corresponding to lower concentrations and lower temperatures, as shown in the left panel of Fig. 15) and from configurations in the cubic phase without microstructure (open circles, corresponding to higher concentrations and higher temperatures, as shown in the

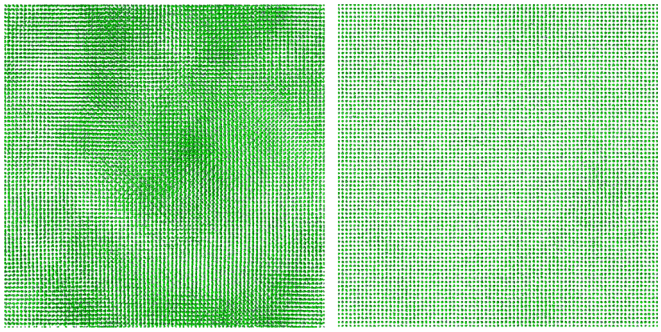

FIG. 15. Structure of ZrO_2 with 16% of yttrium (zirconium is colored in green and yttrium is in grey), at 1000 K (left) and 1800 K (right). The structure transforms to the cubic phase entirely when temperatures increase to 1800 K.

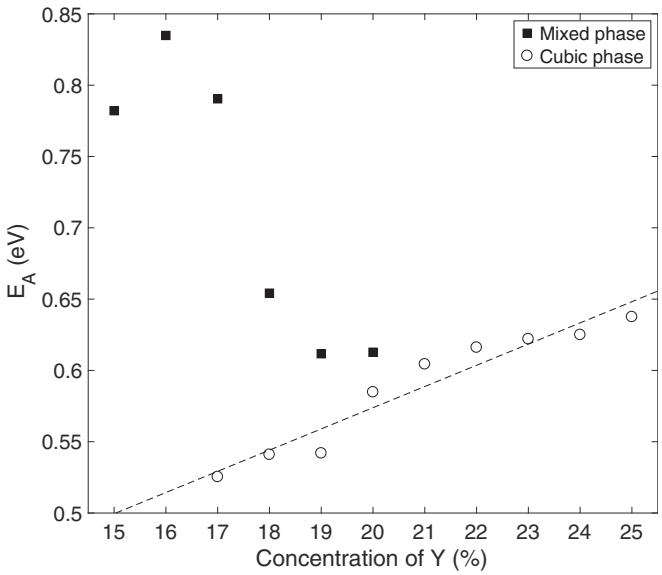

FIG. 16. Dependence of the effective activation energy of oxygen diffusion, obtained from the slope of the plot of $\ln D$ vs $1/T$ on the concentration of yttrium. The data represented by the open circles were calculated in the system that only contained the cubic structure.

right panel of Fig. 15). As can be seen, for the configurations without microstructure the activation energy increases almost linearly with the concentration of yttrium. This is similar to the result from other simulation studies of the cubic phase [19,25]. However, with microstructure, the effective activation energy begins from the much higher value of around 0.8 eV and decreases quickly with the concentration of yttrium as the concentration of the cubic phase increases, eventually reaching the value of approximately 0.6 eV as in the pure cubic phase.

In summary, we have observed a strong correlation between the existence of microstructure and both the overall diffusivity of oxygen ions and the effective activation energy for diffusion of oxygen in $Zr_{1-x}Y_xO_{2-x/2}$. The correlation has been demonstrated through changes in both yttrium concentration and temperature. In particular, by identifying the correlation with microstructure through changing temperature at fixed yttrium concentration x we have demonstrated that the correlation between diffusion and x arises indirectly from the dependence of microstructure on x at any fixed temperature. This may explain why many diffusion simulations give a complicated and often unclear picture of what governs the activation energy [12,13], particularly if smaller sizes of simulation configurations constrain the emergence of microstructures.

IV. CONCLUSIONS

In this paper we have quantified and characterized the microstructure of $Zr_{1-x}Y_xO_{2-x/2}$ using molecular dynamics simulation. To enable the natural emergence of microstructure without constraining the shape and size of the simulation sample it is essential to perform simulations of very large systems, which we have been able to achieve here. The simulations have shown that for lower concentrations of yttrium the atomic configurations are composed of an interesting microstructure of cubic and orthorhombic coexisting phases, then with the growth of the cubic form and eventual transformation at 18% concentration to a pure cubic form without microstructure. In addition, calculations of oxygen diffusion in the Y-doped ZrO_2 show a strong correlation of both overall diffusivity and effective activation energy with the existence of microstructure. In short, the diffusivity is lower and activation higher with the existence of microstructure between the two coexisting phases.

The key point to emerge from this is that it is now possible to study ionic conductivity of yttrium-doped ZrO_2 with the full microstructure as enabled by modern capabilities to perform very large simulations with many state points (concentration and temperature). In the past, simulations of this scientific problem were limited by sample size, which has been reflected in the divergence of results reported. The main scientific finding has been a strong correlation between microstructure and oxygen ion diffusion, which is important for further development of these and related materials with microstructures.

ACKNOWLEDGMENTS

The molecular dynamics simulations were carried out using the ARCHER UK National Supercomputing Service (http://www.archer.ac.uk), with access made available through our membership of the UK's HEC Materials Chemistry Consortium, which is funded by EPSRC (EP/L000202). C.Y. was supported by both the China Scholarship Council and Queen Mary University of London.

[1] J. Chevalier, L. Gremillard, A. V. Virkar, and D. R. Clarke, J. Am. Ceram. Soc. **92**, 1901 (2009).
[2] M. Yashima, M. Kakihana, and M. Yoshimura, Solid State Ionics **86-88**, 1131 (1996).
[3] N. Mahato, A. Banerjee, A. Gupta, S. Omar, and K. Balani, Prog. Mater. Sci. **72**, 141 (2015).
[4] O. Fabrichnaya and F. Aldinger, Z. Metallkd. **95**, 27 (2004).
[5] J. P. Goff, W. Hayes, S. Hull, M. T. Hutchings, and K. N. Clausen, Phys. Rev. B **59**, 14202 (1999).
[6] S. García-Martín, D. Fagg, and J. Irvine, Chem. Mater. **20**, 5933 (2008).
[7] H. Kim, J. Y. Moon, J.-H. Lee, J.-K. Lee, Y.-W. Heo, J.-J. Kim, and H. S. Lee, J. Nanosci. Nanotechnol. **14**, 7961 (2014).
[8] E. V. Stefanovich, A. L. Shluger, and C. R. A. Catlow, Phys. Rev. B **49**, 11560 (1994).
[9] X. Xia, R. Oldman, and R. Catlow, Chem. Mater. **21**, 3576 (2009).
[10] P. K. Schelling, S. R. Phillpot, and D. Wolf, J. Am. Ceram. Soc. **84**, 1609 (2001).
[11] D. S. Aidhy, Y. Zhang, and W. J. Weber, Phys. Chem. Chem. Phys. **15**, 18915 (2013).
[12] M. Kilo, C. Argirusis, G. Borchardt, and R. a. Jackson, Phys. Chem. Chem. Phys. **5**, 2219 (2003).

[13] X. Li and B. Hafskjold, J. Phys.: Condens. Matter **7**, 1255 (1995).
[14] M. Filal, C. Petot, M. Mokchah, C. Chateau, and J. L. Carpentier, Solid State Ionics **80**, 27 (1995).
[15] P. Manning, Solid State Ionics **100**, 1 (1997).
[16] J. Luo, D. P. Almond, and R. Stevens, J. Am. Ceram. Soc. **83**, 1703 (2000).
[17] D. Marrocchelli, P. A. Madden, S. T. Norberg, and S. Hull, Chem. Mater. **23**, 1365 (2011).
[18] I. R. Gibson and J. T. S. Irvine, J. Mater. Chem. **6**, 895 (1996).
[19] R. Krishnamurthy, Y.-G. Yoon, D. J. Srolovitz, and R. Car, J. Am. Ceram. Soc. **87**, 1821 (2004).
[20] R. Pornprasertsuk, P. Ramanarayanan, C. B. Musgrave, and F. B. Prinz, J. Appl. Phys. **98**, 103513 (2005).
[21] A. J. G. Lunt, M. Y. Xie, N. Baimpas, S. Y. Zhang, S. Kabra, J. Kelleher, T. K. Neo, and A. M. Korsunsky, J. Appl. Phys. **116**, 053509 (2014).
[22] J. D. Gale and A. L. Rohl, Mol. Simul. **29**, 291 (2003).
[23] I. T. Todorov, W. Smith, K. Trachenko, and M. T. Dove, J. Mater. Chem. **16**, 1911 (2006).
[24] D. W. Strickler and W. G. Carlson, J. Am. Ceram. Soc. **47**, 122 (1964).
[25] R. Devanathan, W. J. Weber, S. C. Singhal, and J. D. Gale, Solid State Ionics **177**, 1251 (2006).